Effect of Y3Al5O12 Addition on The Microstructural Evaluation And Mechanical Properties of Spark Plasma Sintered ZrB2-SiC Composites

Kübra Gürcan (kubragurcan@eskisehir.edu.tr)
Eskisehir Teknik Universitesi https://orcid.org/0000-0003-0434-1518
Erhan Ayas
Eskişehir Technical University: Eskisehir Teknik Universitesi
İlker Yurdabak
Eskişehir Technical University: Eskisehir Teknik Universitesi
M.Safa Güngören
Eskişehir Technical University: Eskisehir Teknik Universitesi

Research Article

Keywords: YAG, ZrB2-SiC, UHTC, SPS

Posted Date: November 5th, 2020

DOI: https://doi.org/10.21203/rs.3.rs-101301/v1

Version of Record: A version of this preprint was published at Science of Sintering on January 1st, 2022.
See the published version at https://doi.org/10.2298/SOS2201001G.

Effect of $Y_3Al_5O_{12}$ addition on the microstructural evaluation and mechanical properties of Spark Plasma Sintered ZrB_2-SiC composites

Kübra Gürcan[a*] Erhan Ayas[a] İlker Yurdabak[a] M.Safa Güngören[a]

[a]Department of Material Science & Engineering, Eskişehir Technical University, 26480, Eskişehir/Turkey

ABSTRACT

The addition of $Y_3Al_5O_{12}$ (YAG) into the ZrB_2-SiC composites was investigated in the present research. Composites were densified by SPS method at 1850ºC under a uniaxial pressure of 50 MPa for 20 min. Microstructural evaluation and mechanical properties were evaluated with a various content of YAG (1-5 wt%). The microstructural and phase analysis showed that incorporation of YAG promoted the densification process from the solid-state sintering to liquid phase sintering. The highest density (99.81% RD) and fracture toughness (6,44 ± 0.23 $MPa.m^{1/2}$) were obtained for the composite containing 5 wt % YAG after the SPS process. Although hardness and elastic modulus of samples were decreased with the increasing of YAG amount, measured values were comparable with the literature.

Keywords: YAG, ZrB_2-SiC, UHTC, SPS

Corresponding Author*: Kübra Gürcan

E-mail: kubragurcan@eskisehir.edu.tr

1. INTRODUCTION

Belong the family of Ultra High Temperature Ceramics (UHTCs), transition metal borides like ZrB_2 and HfB_2 have unique combination of thermophysical properties, including high melting temperature, high strength and hardness, high thermal and electrical conductivity and high chemical stability [1-3]. Due to these unique properties, these materials are potential candidates for high temperature applications like propulsion systems, rocket nozzles, re-entry and hypersonic vehicles involving sharp leading edges and nose cones for re-entry and hypersonic vehicles. In order to be manoeuvrable at hypersonic velocities, sharp leading edges and nose cones are required control surfaces. If low radius leading edges are designed, manoeuvrability will be higher. However, formation of much greater aerothermal heating, leading edges part may reach higher temperatures (> 2000°C) during re-entry [4, 5]. The currently used materials will not resist such extreme temperatures and more stable materials are required for use in this type of high temperature applications. In the earlier studies [6-12] ZrB_2-SiC and HfB_2-SiC composites have come to the forefront under these extreme conditions due to their high strength and high stability. Recently, yttrium and aluminium based additives including Al_2O_3, Y_2O_3 have been successfully used to improve the sinterability of ZrB_2, forming a liquid phase or removal of surface oxides. In addition to sinterability, it has been stated that these additions played an important role for improving mechanical properties and oxidation resistance [13-20]. YAG gel coated ZrB_2-SiC composites were prepared by pressureless sintering by He et all [15]. Obtained results showed that coated YAG have led to high relative density (about 97%) at the sintering temperature of 1950°C due to the changing of the sintering mechanism from solid state to liquid phase sintering.

Yttrium aluminium garnet (YAG or $Y_3Al_5O_{12}$) is the only unambiguously stable phase in Y_2O_3-Al_2O_3 system which has a great interest as a high temperature application material as a matrix due to its high temperature strength. In addition to matrix phase, it is used as a sintering agent for some ceramic matrices. To our best knowledge, YAG has been formed during the sintering of ZrB_2 based ceramics using Y_2O_3 and Al_2O_3 addition in the system [16, 21, 22]. However, formation of a single phase YAG with Y_2O_3-Al_2O_3 system is difficult in the high pressure and temperature assisted sintering techniques like SPS, HP. In this research, therefore, commercial YAG powder were added to the ZrB_2-SiC composites consolidated by the spark plasma sintering. The influence of different YAG contents were investigated on the microstructure evaluation and mechanical properties of composites.

2. MATERIALS AND METHOD

2.1. Powder Preparation and SPS of powders

Commercially available ZrB_2 (ABCR GmbH, Grade A), SiC, (HC Starck-UF-05) powders and YAG droplets (ABCR GmbH) were used as starting powders. YAG droplets were first crushed in a ring mill (WC-Co media) and the crushed powders were milled in a planetary ball mill (Pulverisette, P6, Fritsch) for size reduction in a ZrO_2 milling media (10 mm ball diameter and 80 ml jar capacity). Ball to powder ratio was selected as 10:1 and the powders were milled about 120 min at a rotational speed of 450 rpm. In order to minimize cold welding, 0.5 % wt. stearic acid (Merck,Germany) was added as a process control agent. After the milling process, 1, 3 and 5% wt. YAG mixed with ZrB_2-25 vol %SiC composite powders were prepared using the planetary ball mill in a Si_3N_4 media (10mm ball diameter, 250 ml jar capacity) with 2-propanol for 90 min at a rotational speed of 450 rpm. The slurry was then dried using a rotary

evaporator (WB2000, Heidolph) at 50 rpm and 55°C for 1 h. Dried powders were sieved under 100 μm to break up agglomerates.

Sintering of composites was carried out in an SPS furnace (HPD- 50, FCT GmbH, Germany) at 1850°C under a uniaxially pressure of 50 MPa for 20 min. The heating rate was kept constant as 100°C min^{-1}. In every sintering cycle 6 gr of powder was placed into the graphite die with an inner diameter of 20 mm. Graphite foil with a thickness of 1 mm was incorporated inside the die to prevent reaction between the die and powders. The temperature was increased with a controlled electric current and measured on the graphite die surface with an optical pyrometer.

2.2. Characterization of sintered samples

Bulk densities were measured by using Archimedes method after removing the graphite foil layer formed on the sintered sample surfaces. In order to determine relative density values, all theoretical values for ZrB_2-SiC-YAG composites were calculated from volume-based rules of mixtures. The bulk densities of ZrB_2, SiC and YAG were accepted as 6,1 g/cm^3, 3.2 g/cm^3, and 4,56 g/cm^3, respectively. To perform phase analysis, sintered samples were crushed and ground down to 63 μm. The qualitative phase analysis was accomplished by using X-Ray diffractometer (Rigaku MiniFlex600, Japan) between 20 and 80° (2θ) under the conditions of 40 kV accelerating voltage, 15 mA current, 2° min^{-1} scan speed and 0.02 step size. The cross-sections of samples were mirror-like polished (Struers TegraPol-25, Denmark) for microstructural analysis. SEM and quantitative elemental analysis were performed by using a scanning electron microscope (SEM, Supra 50VP, Zeiss, Germany) equipped with backscatter electron (BSE), secondary electron (SE) and energy-dispersive X-ray spectroscopy (EDS) detectors.

For the elastic modulus measurement, sintered samples with the dimension of 20 mm in diameter and 5 mm in thickness were ground to obtain a graphite-free surface and parallel opposite faces of better than 3 µm surface roughness. Before the measurement, sample thickness, h, was measured with micrometer with an accuracy of 1 µm resolution micrometer (Mitutoyo M110-25 DS). Elastic modulus of samples was determined using ultrasonic transducers operating on a pulse-echo mode with a fundamental frequency of 5MHz for longitudinal waves and 2.25 MHz for shear waves. The time of flight measurements for the ultrasonic signals was performed using a digital oscilloscope (Tektronix TDS 1012 Two Channel Digital Storage Oscilloscope). For each of the samples the time of flight of ultrasonic wave measurements were repeated at least 5 times. The Young Modulus (E), Shear modulus (G), bulk modulus (B), and Poisson's ratio (υ), were given by following equations [23]

$$E = \rho V_t^2 \frac{3V_l^2 - 4V_t^2}{V_l^2 - V_t^2}$$

$$G = \rho\, V_t^2$$

$$\upsilon = \frac{E}{2G} - 1$$

where ρ indicates the density, V_l and V_t are the longitudinal and transverse sound wave velocities, respectively, and the V_l and V_t are determined by;

$$V_l = \frac{2h}{\Delta t_l}$$

$$V_t = \frac{2h}{\Delta t_t}$$

where Δt_l and Δt_t are the elapsed times between the pulse and the echo of the longitudinal and transverse waves, respectively.

The Vicker Hardness (Hv) was measured from the polished cross-sectional surface of samples using an indenter (EMCO Test, M1C, Germany) under a load of 10 kg applied for 3 s. At least three indentations were applied for each sample and average values were calculated for statistical results. The Vickers hardness (HV) values were determined by the following equation [24].

$$HV = \frac{2Psin\theta}{d^2} = \frac{1.8544P}{d^2}$$

Where P is applied load (kgf), θ was the apical angle of indenter (136°) and d was the average size of two diagonals of the indentation impression (mm). The fracture toughness (K_{IC}) of samples was determined by indentation fracture (IF) method. Following the micro-hardness test, the lengths of radial cracks were measured which had formed in the corners of the Vickers indentation mark on the surface. Next, the most used empirical equation proposed by Evans [25] was used to calculate fracture toughness values, which is following:

$$K_{IC} = 0.16\,(\frac{c}{a})^{-1.5}\,(H)(a^{\frac{1}{2}})$$

where K_{IC} is fracture toughness ($MPa.m^{1/2}$), H is Vickers hardness (MPa), c is the average length of the cracks (μm), and α is the half average length of the diagonal (μm).

3. RESULT AND DISCUSSIONS

3.1. Phase and Microstructural Analysis of Sintered Samples

The morphology and XRD patterns of the milled YAG powder were given in **Fig.1.** According to the **Fig.1.b** the XRD patterns of the YAG powder indicated the existence of $Y_3Al_5O_{12}$ (PDF-JCPDS 33-0040) peaks and $YAlO_3$(PDF-JCPDS 33-0041), the perovskite-like form of yttrium aluminium oxide phases. SE-SEM micrographs of YAG powders exhibited spherical form with a mean particle size of < 2 μm **(Fig.1.a)**.

The XRD patterns of the all the sintered samples were given in **Fig. 2**. No new phases were detected apart from ZrB_2 (PDF-JCPDS 34-0423), α-SiC (PDF-JCPDS 29-1131) and YAG (PDF-JCPDS 09-0310). Bragg reflections with those of the SiC and YAG were significantly overlapped, convenient with the literature.[26]. **Fig. 2.b** illustrated the XRD patterns of all samples between 20 and 45º. The unit cell parameters of 1,3, and 5% wt YAG included samples were calculated as a=3.1636 Aº c=3.5260 Aº, a=3.1655 Aº c=3.5273 Aº and a=3.1583 Aº, c=3.5163 Aº, respectively. These values were lower than those of pure ZrB_2 (a=3.1687 Aº, c=3.5300 Aº). This was a result of Y substitution for Zr in the unit cell with compensation anion vacancies due to the similar atomic diameters between Zr and Y. This result was also in agreement with the findings of Ingel and Lewis[27].

The BSE-SEM images for the polished surfaces of all sintered samples were presented in **Fig.3.** In all figures, bright contrasted areas were related to ZrB_2, the dark areas attributed to SiC, and the grey areas at the interface of ZrB_2-SiC belong to YAG phases as confirmed with EDX. SiC and YAG phases were homogeneously distributed around the ZrB_2 grains and no agglomeration was detected. Due to the internal residual stresses formed during SPS, pull out defects

(indicated as yellow arrows on the image) were observed in the microstructures. The measured relative densities of the samples densified at 1850ºC **(Table 1)** were in the range of 98-100% of the true densities, and nearly full densification was obtained in sample ZrB_2-SiC-5YAG. The SEM images of fracture surfaces of ZrB_2-SiC and ZrB_2-SiC-5YAG were given in **Fig.4.** Consistent with the calculated density values, there were still remaining porosities in the microstructure of the fracture surface of ZrB_2-SiC sample shown by arrows. On the other hand, ZrB_2-SiC-5YAG sample was very scarce residual porosity. Consistent with the literature [15], joule heating from the pulse current led to melting of YAG particles and it promoted the sintering type of ZrB_2-SiC from the solid-state sintering to liquid phase sintering during the SPS. Due to the high grain boundary in liquid phase sintering, YAG was thought to cause grain growth of both ZrB_2 and SiC grains in the sintered samples, especially ZrB_2-SiC-5YAG**. Fig. 4.b** also showed that ZrB_2-SiC-5YAG sample exhibited the intercrystalline cracking characteristic which promoted the higher fracture toughness.

3.2. Mechanical properties of sintered samples

Hardness, fracture toughness and elastic modulus of sintered samples as a function of YAG content were indicated in **Fig.5.** A fracture toughness of 4.87 ± 0.21 $MPa.m^{1/2}$ was measured for ZrB_2-SiC composite, increased after the addition of YAG. The highest fracture toughness was obtained for the composite containing 5 wt% YAG with a value of 6,44 ± 0.23 $MPa.m^{1/2}$. The toughness values were higher to the result of He et all [15] who reported toughness value of 4.13 ± 0.45 $MPa.m^{1/2}$ for presureless sintered ZrB_2-SiC-YAG composite. Cracks propagate in the material predominantly by an intercrystalline mechanism **(Fig. 4.b),** with separate grains fractured by a transcrystalline mechanism for ZrB_2-SiC-5YAG sample. The crack path created by the Vickers indentation tests for the ZrB_2-SiC-5YAG sample was illustrated in **Fig.6.**

Inspection of the crack propagation revealed crack deflection and crack bridging in ZrB_2-SiC-5YAG sample. These toughening mechanisms increased energy dissipation during the crack propagation and thereby raising fracture toughness. Also, mismatch of the thermal expansion coefficient between SiC, YAG and ZrB_2 could also produce tensile stress on grain boundaries in the ZrB_2, leading to the formation of microcracks as shown with red arrows in **Fig.6.** The microcracks dissipated the deformation energy and decreased the stress intensity of the main crack and thereby improving the fracture toughness of the material.

As it was well known that fine grained materials have high hardness, which was supported by much research [28-30]. With the addition of YAG, the hardness of samples decreased from 18.74 ± 0.43 GPa to 16.71 ± 0.55 GPa **(Fig.5.a)** because of the increase of volume fraction of YAG, which is lower hardness than do ZrB_2 and SiC grains. As for the lowest values of hardness in ZrB_2-SiC-5YAG, it was also due to larger grain size, clearly observed in **Fig. 3.d.**

The elastic modulus E of the samples with YAG additives ranged from 512.13 GPa to 458.97 GPa which was lower than ZrB_2-SiC without YAG (528,13 GPa). As it was well known that, density and grain boundary phases were the two major factors that influence E value of the materials. As all samples with the YAG added had a relative density greater than 98% RD, thus, the value of E has been dominated by the secondary phase. Similar to hardness results, elastic modulus of YAG is lower than ZrB_2-SiC matrix, which resulted in a decrease of those of composites with increasing of YAG content. Also, it was thought that the decline in the elastic modulus was due to the formation of microcracks caused by the mismatch of thermal expansion of ZrB_2-SiC and YAG phases.

4. CONCLUSION

YAG added ZrB_2-25 vol%SiC composites were formed by SPS route at 1850ºC under pressure of 50 MPa for 20 min. Effect of YAG amount on the microstructural evaluation and mechanical properties were investigated in detail. After the sintering main phases were detected as ZrB_2, SiC and YAG. It was observed that YAG addition changed the densification process from solid state sintering to liquid phase sintering. Nearly full density was obtained with the addition of 5%wt YAG. Although densification level was increased, grain growth of ZrB_2 and SiC grains were also observed due to the increasing grain boundary mobility. Although grain growth caused a decline on the hardness and elastic modulus, obtained values were comparable with the literature. Fracture toughness of sample was enhanced with the increasing of the YAG addition. Higher fracture toughness about 6,44 ± 0.23 $MPa.m^{1/2}$ was obtained for the 5 vol% YAG added composites. Crack deflection, crack bridging and formation of microcracks were the main toughening mechanisms for this sample.

5. REFERENCES

[1] Wuchina E, Opeka M, Causey S, Buesking K, Spain J, Cull A, et al. Designing for ultrahigh-temperature applications: The mechanical and thermal properties of HfB2, HfCx, HfNxand αHf(N). Journal of Materials Science. 2004;39:5939-49.

[2] Wuchina E, Opila E, Opeka M, Fahrenholtz W, Talmy I. UHTCs: Ultra-High Temperature Ceramic materials for extreme environment applications. Electrochemical Society Interface. 2007;16:30-6.

[3] Fahrenholtz WG. A Historical Perspective on Research Related to Ultra-High Temperature Ceramics. In: W. G. Fahrenholtz EJW, W. E. Lee and Y. Zhou, editor. Ultra-High Temperature Ceramics2014. p. 6-32.

[4] Opeka MM, Talmy IG, Zaykoski JA. Oxidation-based materials selection for 2000°C + hypersonic aerosurfaces: Theoretical considerations and historical experience. Journal of Materials Science. 2004;39:5887-904.

[5] Van Wie DM, Drewry DG, King DE, Hudson CM. The hypersonic environment: Required operating conditions and design challenges. Journal of Materials Science. 2004;39:5915-24.

[6] Chamberlain AL, Fahrenholtz WG, Hilmas GE, Ellerby DT. High-Strength Zirconium Diboride-Based Ceramics. Journal of the American Ceramic Society. 2004;87:1170-2.

[7] Chamberlain A, Fahrenholtz W, Hilmas G, Ellerby D. Oxidation of ZrB2-SiC ceramics under atmospheric and reentry conditions. Refract Appl Trans. 2005;1:1-8.

[8] Carney CM, Key TS. Comparison of the Oxidation Protection of HfB2 Based Ultra-High Temperature Ceramics by the Addition of SiC or MoSi2. Ceramic Engineering and Science Proceedings. 2014;35:261-73.

[9] Monteverde F. Ultra-high temperature HfB2–SiC ceramics consolidated by hot-pressing and spark plasma sintering. Journal of Alloys and Compounds. 2007;428:197-205.

[10] Monteverde F, Melandri C, Guicciardi S. Microstructure and mechanical properties of an HfB2+30vol.% SiC composite consolidated by spark plasma sintering. Materials Chemistry and Physics. 2006;100:513-9.

[11] Monteverde F. Progress in the fabrication of ultra-high-temperature ceramics: “in situ” synthesis, microstructure and properties of a reactive hot-pressed HfB2–SiC composite. Composites Science and Technology. 2005;65:1869-79.

[12] Zhang H, Jayaseelan DD, Bogomol I, Reece MJ, Hu C, Grasso S, et al. A novel microstructural design to improve the oxidation resistance of ZrB2-SiC ultra-high temperature ceramics (UHTCs). Journal of Alloys and Compounds. 2019;785:958-64.

[13] Krishnarao RV, Bhanuprasad VV, Madhusudhan Reddy G. ZrB2–SiC based composites for thermal protection by reaction sintering of ZrO2+B4C+Si. Journal of Advanced Ceramics. 2017;6:320-9.

[14] Mohammadpour B, Ahmadi Z, Shokouhimehr M, Shahedi Asl M. Spark plasma sintering of Al-doped ZrB2–SiC composite. Ceramics International. 2019;45:4262-7.

[15] He R, Zhang X, Hu P, Han W, Hong C. Preparation of YAG gel coated ZrB2–SiC composite prepared by gelcasting and pressureless sintering. Composites Part B: Engineering. 2013;54:307-12.

[16] Song JG, Li JG, Song JR, Zhang LM. Preparation of high-density YAG/ZrB2 multi-phase ceramics by spark plasma sintering. Journal of Ceramic Processing Research. 2007;8:356-8.

[17] Jie-Guang S, Ming-Han X, Shi-Bin L, Shi-Zhe L, Ting-Ting X, Yao-Qi L, et al. Influence of sintering technology on microstructure and mechanical properties of ZrB2-YAG-Al2O3 ceramics. 2016 5th International Conference on Environment, Materials, Chemistry and Power Electronics: Atlantis Press; 2016.

[18] Song J-G. Oxidation Behavior of ZrB2–YAG–Al2O3 Ceramics at High Temperature. Materials and Manufacturing Processes. 2010;25:724-9.

[19] Samanta AK, Dhargupta KK, De AK, Ghatak S. SiC–YAG sintered composites from hydroxy hydrogel powder precursors. Ceramics International. 2000;26:831-8.

[20] He J, Wang Y, Luo L, An L. Oxidation behaviour of ZrB2–SiC (Al/Y) ceramics at 1700 °C. Journal of the European Ceramic Society. 2016;36:3769-74.

[21] Krishnarao RV, Madhusudhan reddy G. Joining of Cf-SiC composites and ZrB2-SiC based composites for ultra high temperature applications. Ceramics International. 2018;44:10569-78.

[22] Zhu T, Xu L, Zhang X, Han W, Hu P, Weng L. Densification, microstructure and mechanical properties of ZrB2–SiCw ceramic composites. Journal of the European Ceramic Society. 2009;29:2893-901.

[23] Guo S, Hirosaki N, Yamamoto Y, Nishimura T, Mitomo M. Hot-pressed silicon nitride ceramics with Lu2O3 additives: elastic moduli and fracture toughness. Journal of the European Ceramic Society. 2003;23:537-45.

[24] Elssner G, Hoven H, Kiessler G, Wellner P, Wert R. Chapter 6 - Analysis of hardness testing indentations. In: Elssner G, Hoven H, Kiessler G, Wellner P, Wert R, editors. Ceramics and Ceramic Composites. New York: Elsevier Science; 1999. p. 144-58.

[25] Evans AG, Charles EA. Fracture Toughness Determinations by Indentation. Journal of the American Ceramic Society. 1976;59:371-2.

[26] Ortiz AL, Sánchez-Bajo F, Hernández-Jiménez A, Guiberteau F, Cumbrera FL. X-ray line-broadening study of a liquid-phase-sintered silicon carbide. Journal of the European Ceramic Society. 2002;22:2677-87.

[27] Ingel RP, Iii DL. Lattice Parameters and Density for Y2O3-Stabilized ZrO2. Journal of the American Ceramic Society. 1986;69:325-32.

[28] Jaberi Zamharir M, Shahedi Asl M, Ghassemi Kakroudi M, Pourmohammadie Vegan, Jaberi Zamharir M. Significance of hot pressing parameters and reinforcement size on sinterability and mechanical properties of ZrB2–25vol% SiC UHTCs. Ceramics International. 2015;41:9628-36.

[29] Mashhadi M, Khaksari H, Safi S. Pressureless sintering behavior and mechanical properties of ZrB2–SiC composites: effect of SiC content and particle size. Journal of Materials Research and Technology. 2015;4:416-22.

[30] Sciti D, Bellosi A. Effects of additives on densification, microstructure and properties of liquid-phase sintered silicon carbide. Journal of Materials Science. 2000;35:3849-55.

TABLES

Table 1. The measured bulk and relative densities of ZrB_2-SiC-YAG composites

Composites	Bulk density (g/cm^3)	Relative density (g/cm^3)
ZrB_2-SiC	5.28	98,14
ZrB_2-SiC-1YAG	5.31	98,33
ZrB_2-SiC-3YAG	5.33	98,70
ZrB_2-SiC-5YAG	5.39	99,81

FIGURE CAPTIONS

Fig.1. a) The morphology and b) XRD patterns of the milled YAG powder

Fig.2. XRD patterns of all sintered samples a) 20-80º and b) 20-45º 2θ range

Fig.3. BSE-SEM images for the polished surfaces of a) ZrB_2-SiC b) ZrB_2-SiC-1YAG c) ZrB_2-SiC-3YAG and d) ZrB_2-SiC-5YAG sintered samples

Fig.4. The SEM images of fracture surfaces of a) ZrB_2-SiC and b) ZrB_2-SiC-5YAG samples

Fig.5. a) Hardness & Fracture toughness and b) Elastic modulus of sintered samples as a function of YAG content.

Fig.6. The crack path created by the Vickers indentation tests for the ZrB_2-SiC-5YAG sample.

Figures

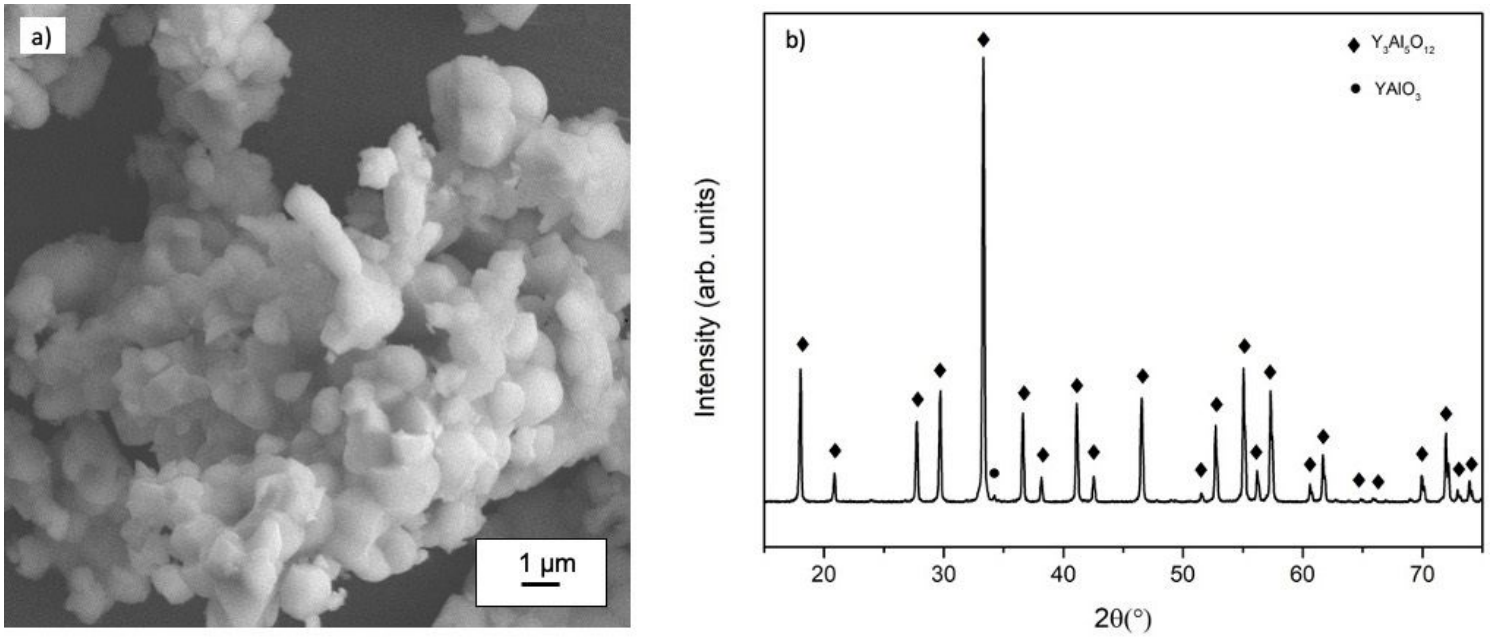

Figure 1

a) The morphology and b) XRD patterns of the milled YAG powder

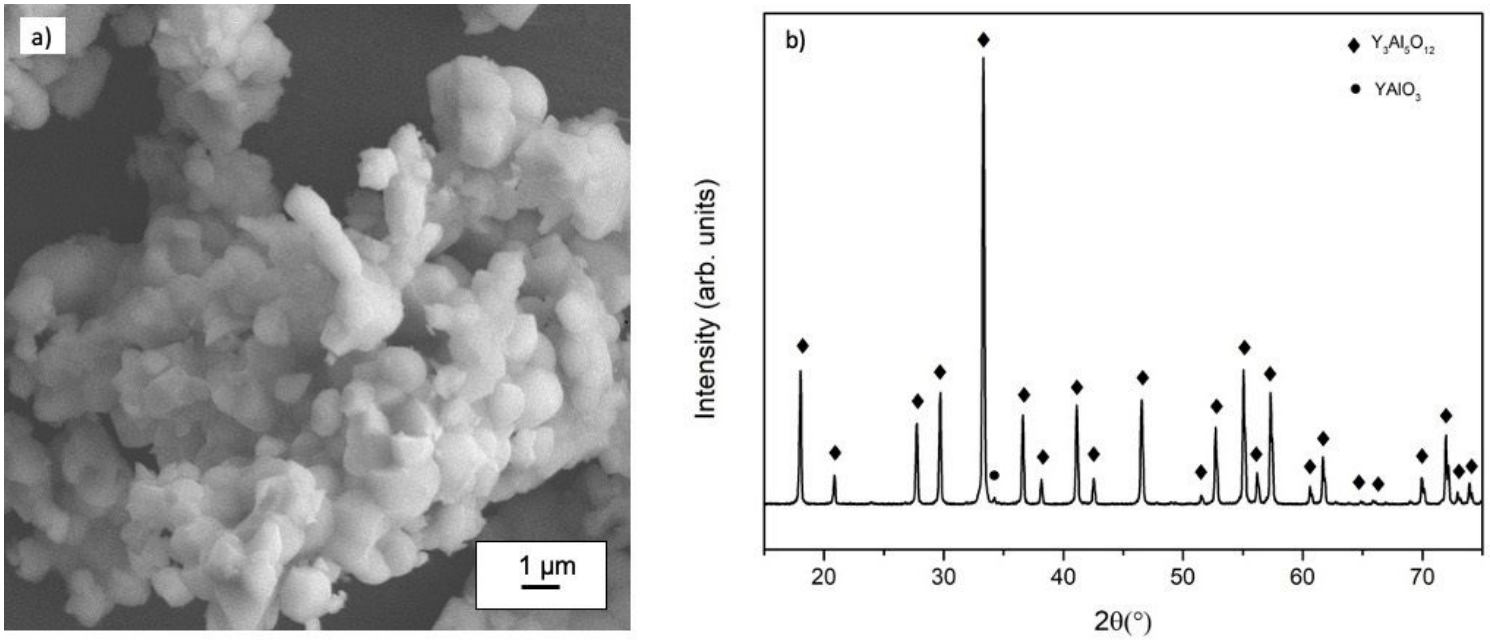

Figure 1

a) The morphology and b) XRD patterns of the milled YAG powder

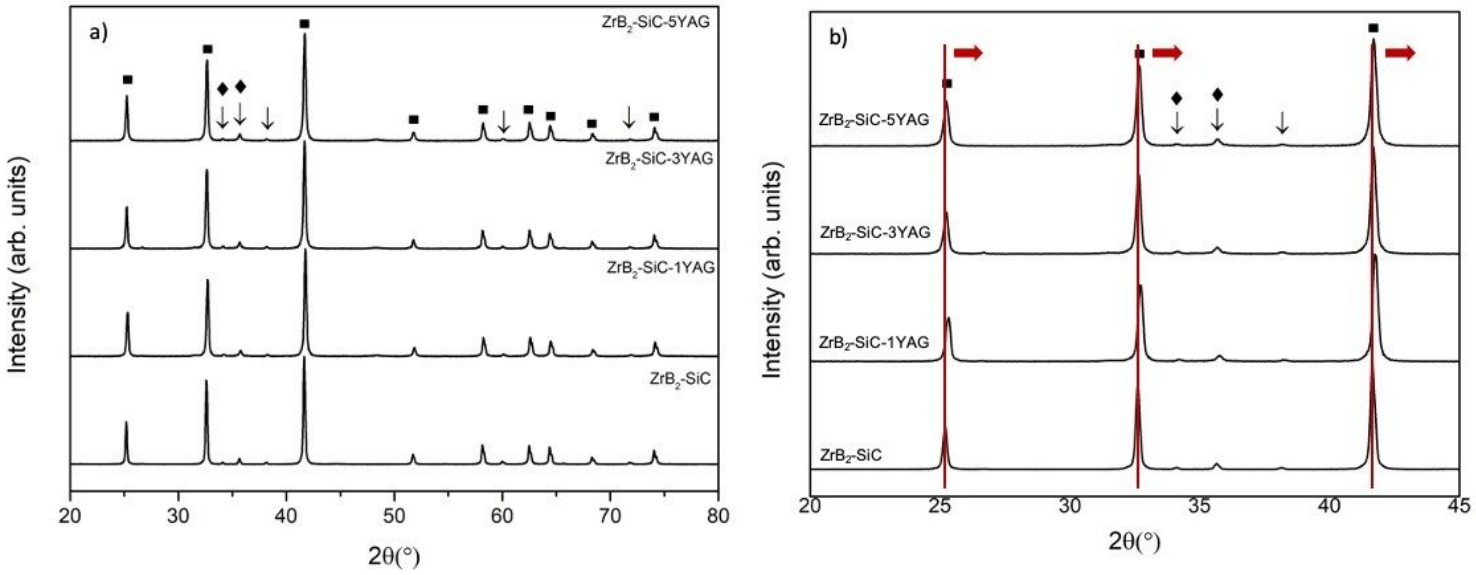

Figure 2

XRD patterns of all sintered samples a) 20-80º and b) 20-45º 2θ range

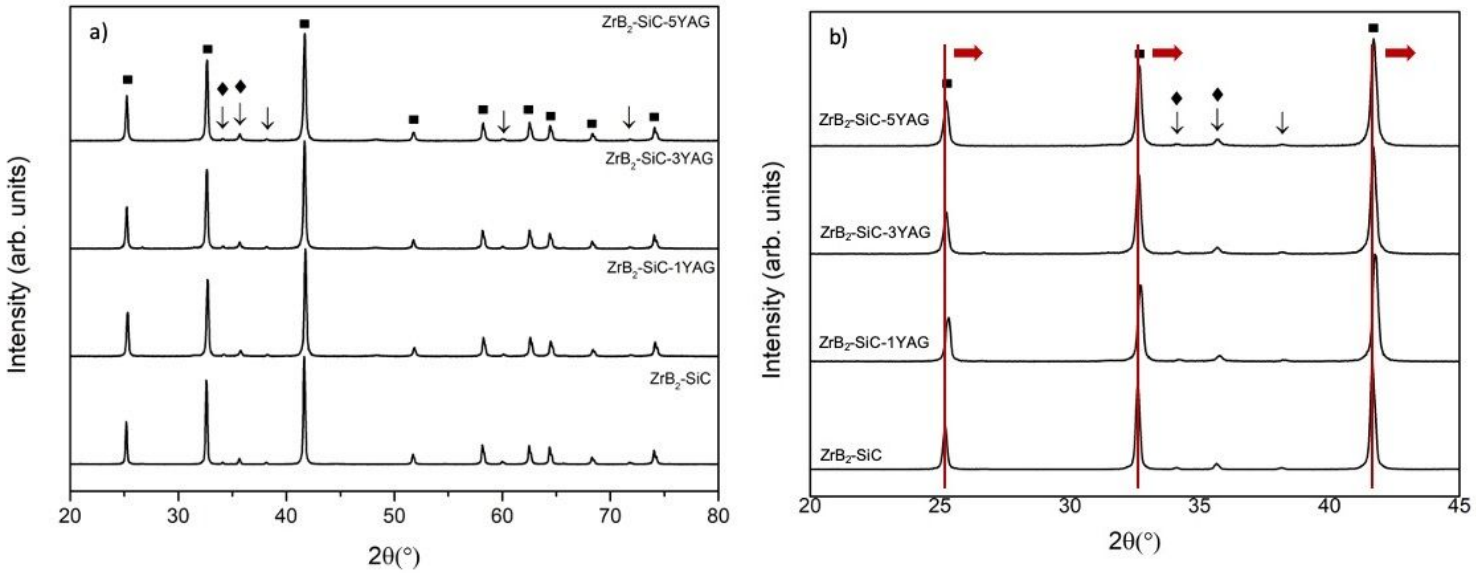

Figure 2

XRD patterns of all sintered samples a) 20-80º and b) 20-45º 2θ range

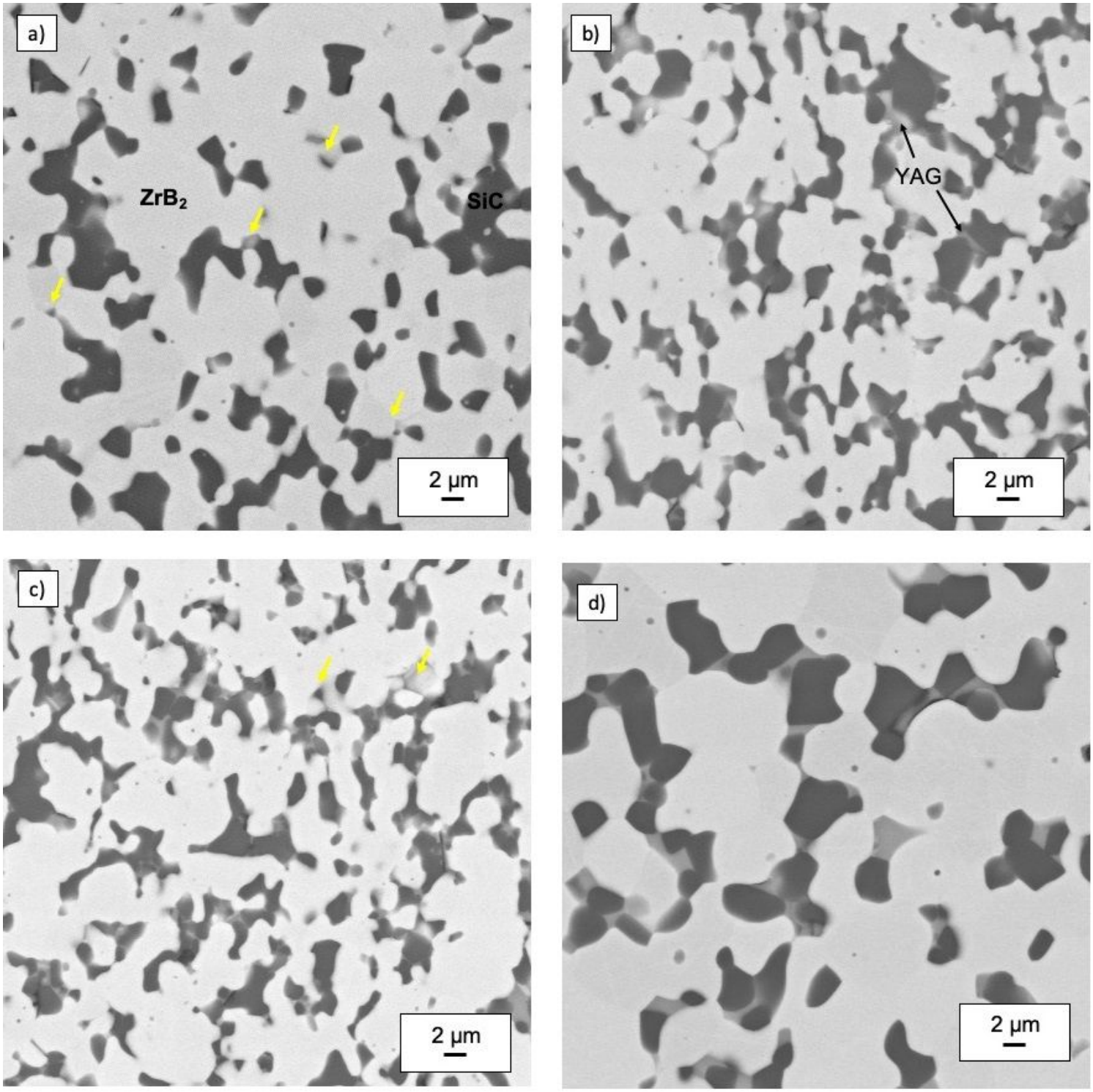

Figure 3

BSE-SEM images for the polished surfaces of a) ZrB2-SiC b) ZrB2-SiC-1YAG c) ZrB2-SiC-3YAG and d) ZrB2-SiC-5YAG sintered samples

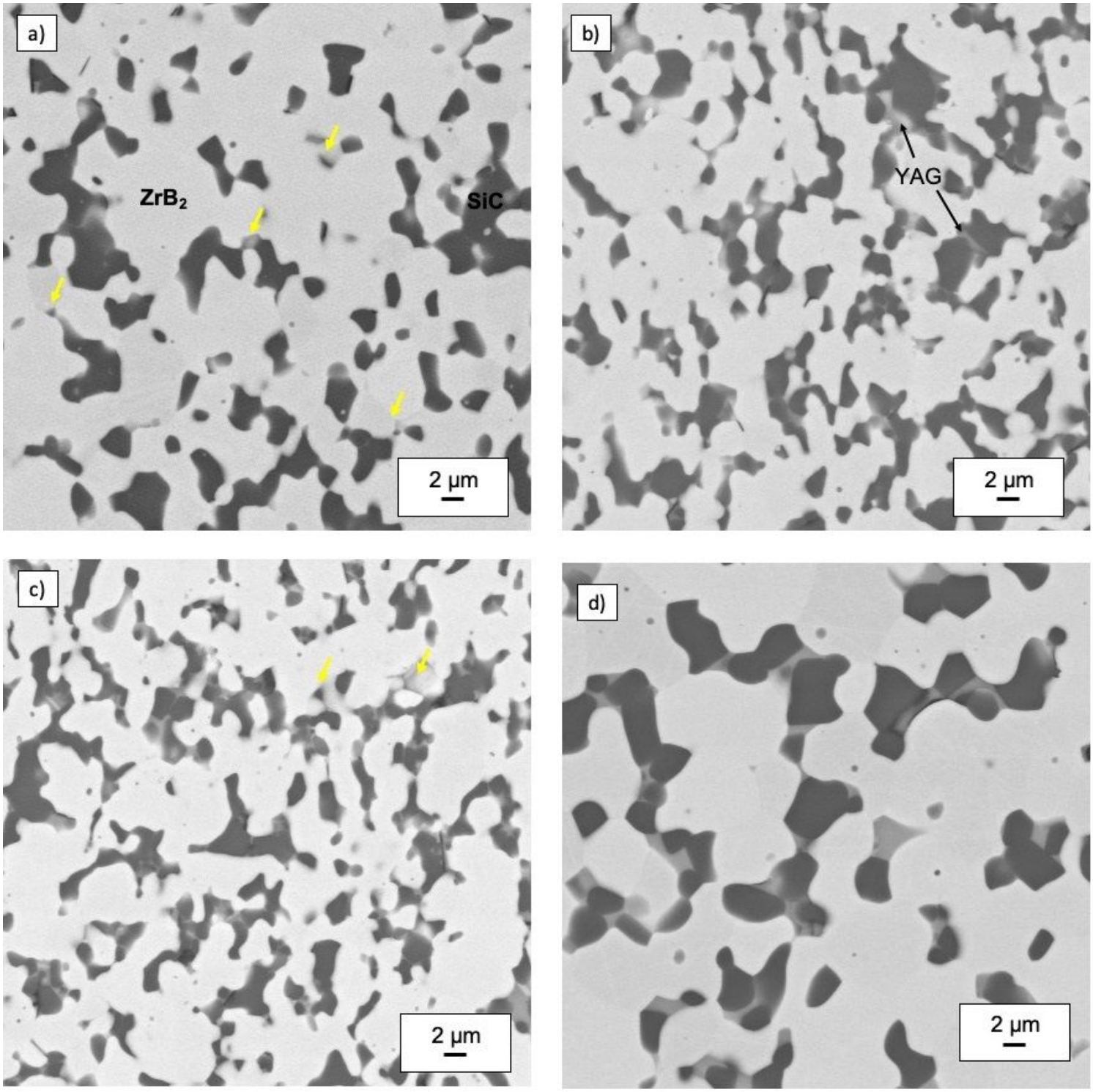

Figure 3

BSE-SEM images for the polished surfaces of a) ZrB2-SiC b) ZrB2-SiC-1YAG c) ZrB2-SiC-3YAG and d) ZrB2-SiC-5YAG sintered samples

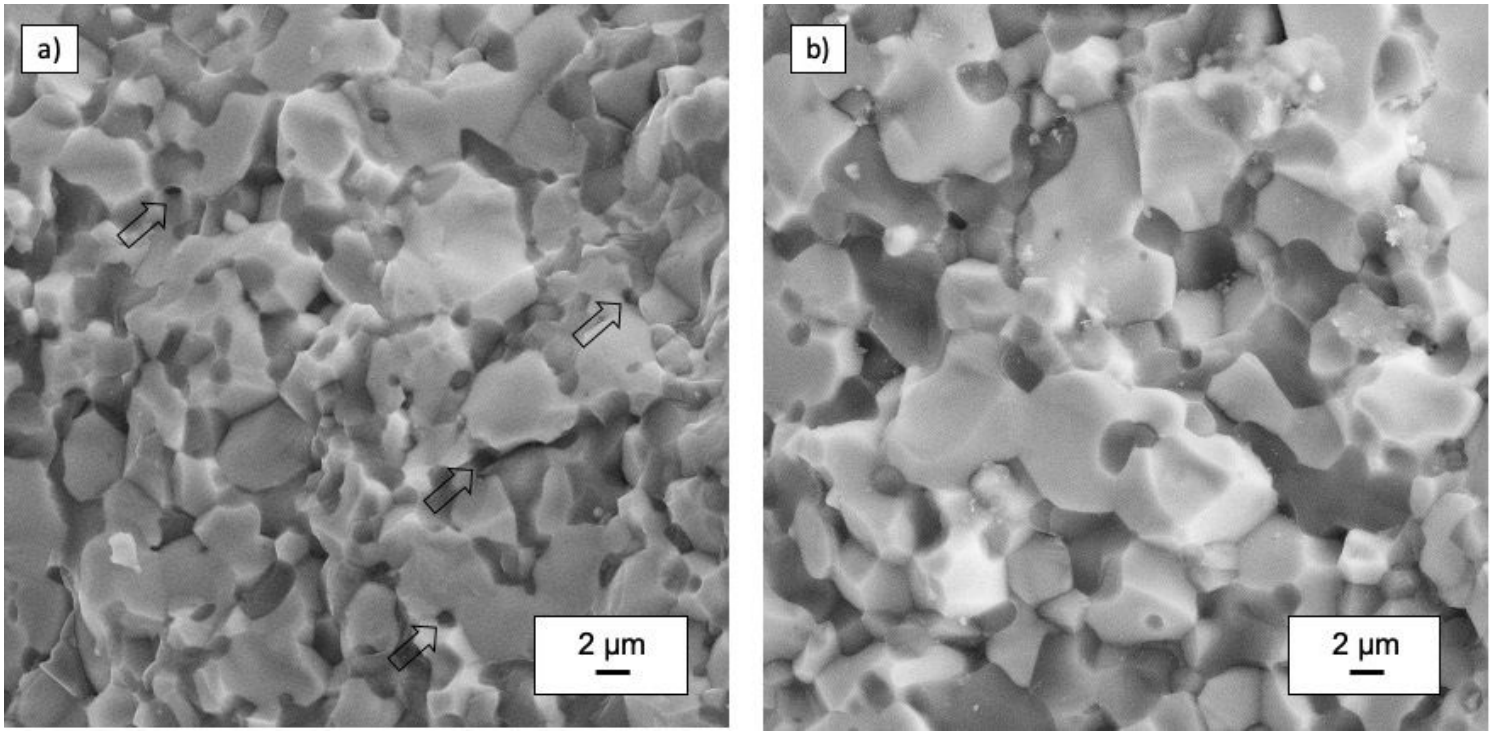

Figure 4

The SEM images of fracture surfaces of a) ZrB2-SiC and b) ZrB2-SiC-5YAG samples

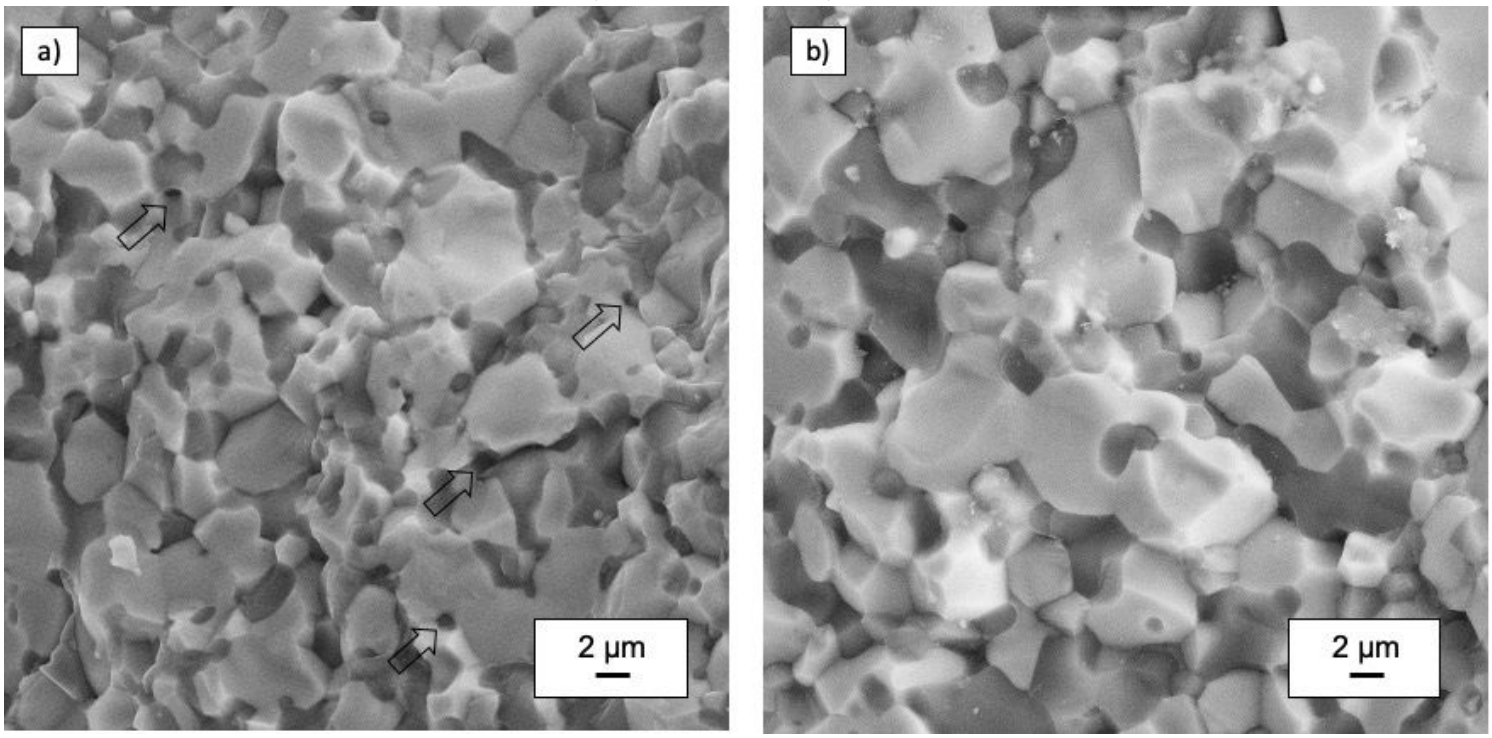

Figure 4

The SEM images of fracture surfaces of a) ZrB2-SiC and b) ZrB2-SiC-5YAG samples

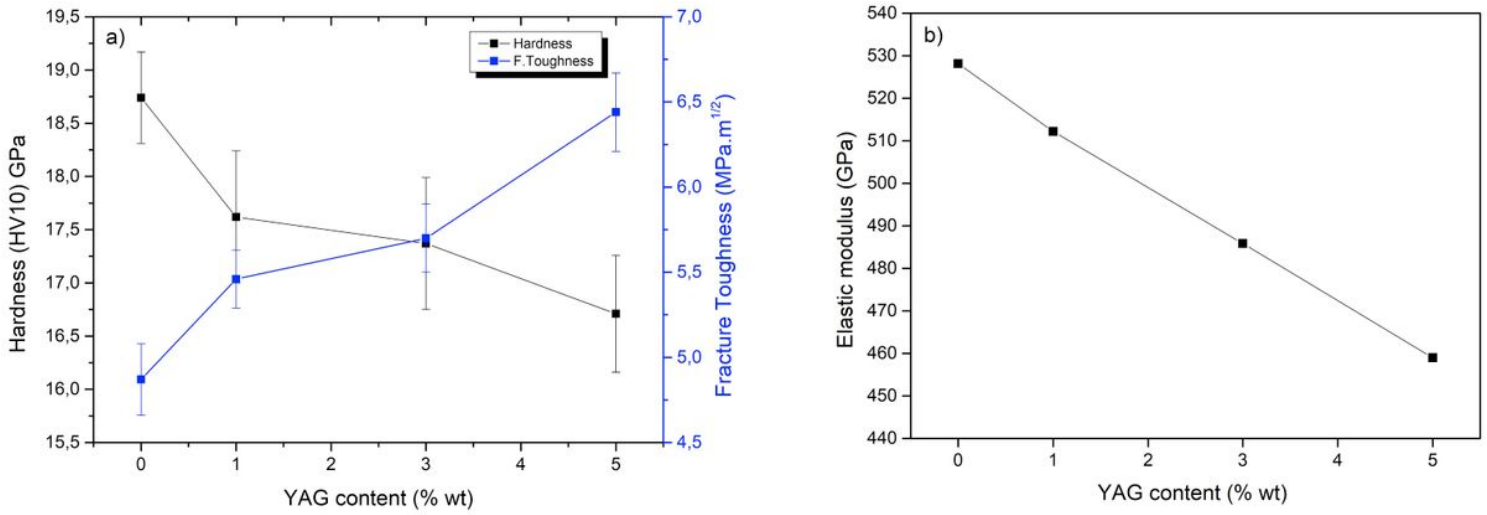

Figure 5

a) Hardness & Fracture toughness and b) Elastic modulus of sintered samples as a function of YAG content.

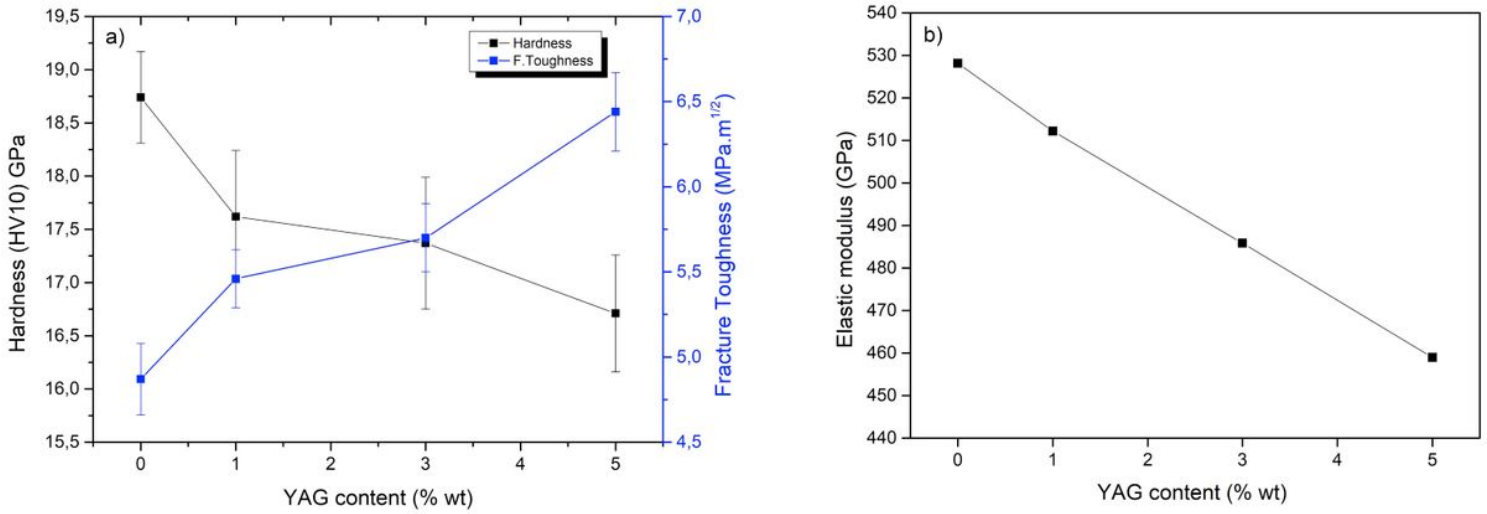

Figure 5

a) Hardness & Fracture toughness and b) Elastic modulus of sintered samples as a function of YAG content.

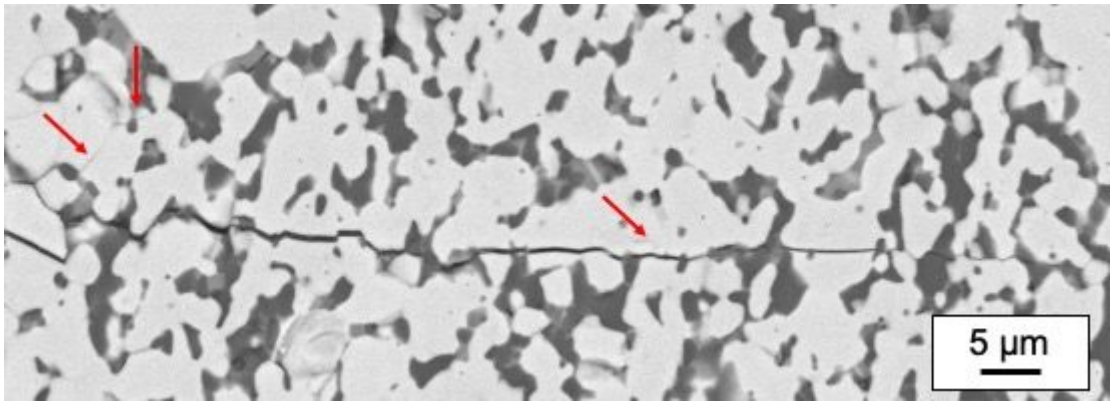

Figure 6

The crack path created by the Vickers indentation tests for the ZrB2-SiC-5YAG sample.

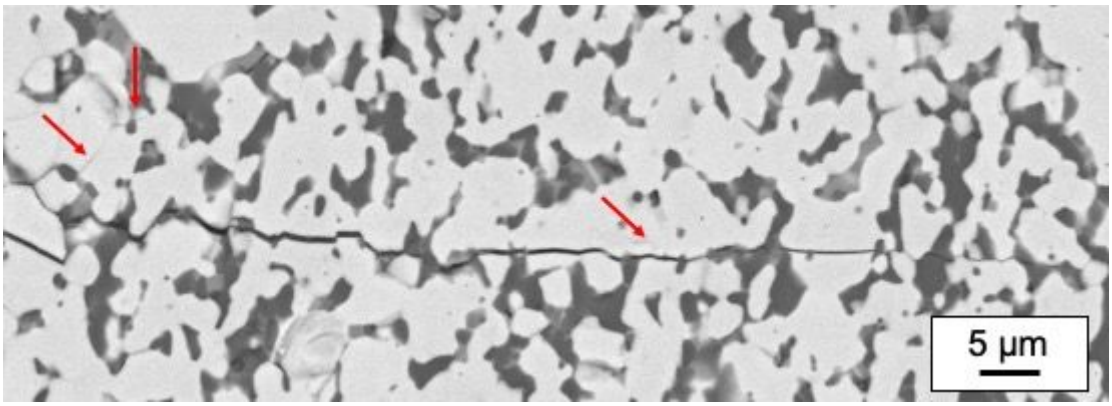

Figure 6

The crack path created by the Vickers indentation tests for the ZrB2-SiC-5YAG sample.